Extremely Vivid, Highly Transparent, and Ultrathin Quantum Dot Light-Emitting Diodes

Moon Kee Choi, Jiwoong Yang, Dong Chan Kim, Zhaohe Dai, Junhee Kim, Hyojin Seung, Vinayak S. Kale, Sae Jin Sung, Chong Rae Park, Nanshu Lu, Taeghwan Hyeon, and Dae-Hyeong Kim**

Displaying information on transparent screens offers new opportunities in next-generation electronics, such as augmented reality devices, smart surgical glasses, and smart windows. Outstanding luminance and transparency are essential for such "see-through" displays to show vivid images over clear background view. Here transparent quantum dot light-emitting diodes (Tr-QLEDs) are reported with high brightness (bottom: ≈43 000 cd m^{-2}, top: ≈30 000 cd m^{-2}, total: ≈73 000 cd m^{-2} at 9 V), excellent transmittance (90% at 550 nm, 84% over visible range), and an ultrathin form factor (≈2.7 µm thickness). These superb characteristics are accomplished by novel electron transport layers (ETLs) and engineered quantum dots (QDs). The ETLs, ZnO nanoparticle assemblies with ultrathin alumina overlayers, dramatically enhance durability of active layers, and balance electron/hole injection into QDs, which prevents nonradiative recombination processes. In addition, the QD structure is further optimized to fully exploit the device architecture. The ultrathin nature of Tr-QLEDs allows their conformal integration on various shaped objects. Finally, the high resolution patterning of red, green, and blue Tr-QLEDs (513 pixels $in.^{-1}$) shows the potential of the full-color transparent display.

Dr. M. K. Choi, Dr. J. Yang, D. C. Kim, J. Kim, H. Seung, V. S. Kale, Prof. T. Hyeon, Prof. D.-H. Kim
Center for Nanoparticle Research
Institute for Basic Science (IBS)
Seoul 08826, Republic of Korea
E-mail: thyeon@snu.ac.kr; dkim98@snu.ac.kr

Dr. M. K. Choi, Dr. J. Yang, D. C. Kim, J. Kim, H. Seung, V. S. Kale, Prof. T. Hyeon, Prof. D.-H. Kim
School of Chemical and Biological Engineering
Institute of Chemical Processes
Seoul National University
Seoul 08826, Republic of Korea

Z. Dai, Prof. N. Lu
Center for Mechanics of Solids
Structures and Materials
Department of Aerospace Engineering and Engineering Mechanics
Department of Biomedical Engineering
Texas Materials Institute
University of Texas at Austin
Austin, TX 78712, USA

S. J. Sung, Prof. C. R. Park
Research Institute of Advanced Materials
Department of Materials Science and Engineering
Seoul National University
Seoul 08826, Republic of Korea

DOI: 10.1002/adma.201703279

Transparent displays lie at the heart of next generation optoelectronics[1,2] in the era of augmented reality (AR), wearable electronics, and internet of things (IoTs).[3–7] Being transparent for light-emitting diodes (LEDs) significantly expands their applications by displaying visual information on objects without affecting their original appearance and functionality. However, there has been a large gap in the electroluminescence (EL) performance between transparent displays and non-transparent counterparts,[8] due in large part to imbalanced injection of charge carriers into the emitter, unoptimized energy band alignment of the top electrode, and vulnerability of organic and/or polymeric light emitting materials during the deposition of transparent conducting oxide electrodes.[9–12] The previous progresses and unmet requirements for transparent displays are described in Section S2.1, Figure S1, and Table S1 of the Supporting Information. In addition, there has been much need to develop novel device architectures[13–16] that consider the carrier dynamics for high-performance transparent quantum dot light-emitting diodes (Tr-QLEDs).

For high-quality transparent displays, first of all, high transparency is an absolute requirement.[17] The effect of transparency on visibility of background is examined on the university logo and a leaf (**Figure 1**a). For transparency below 70% (semitransparency), the color and contrast of objects behind the display are significantly deteriorated. In contrast, Tr-QLEDs of 84% transparency present clear background view in both cases. Secondly, high brightness and color purity are particularly important for vividness of "see-through" displays. The maximum brightness of conventional displays (e.g., smart phones and monitors) is around 600 cd m^{-2}. For see-through displays, however, the displayed information becomes blurred at this brightness (i.e., 600 cd m^{-2}) because of photointerference with ambient light (Figure 1b; Figure S2a, Supporting Information). Therefore, significantly higher brightness is required to ensure clear and vivid displays (Figure 1b). In addition, chromatic aberrations can be minimized by employing engineered quantum dots (QD) emitters[18,19] that exhibit better color purity than organic and/or polymer emitters (Figure S2b, Supporting Information). Lastly, integration of highly deformable

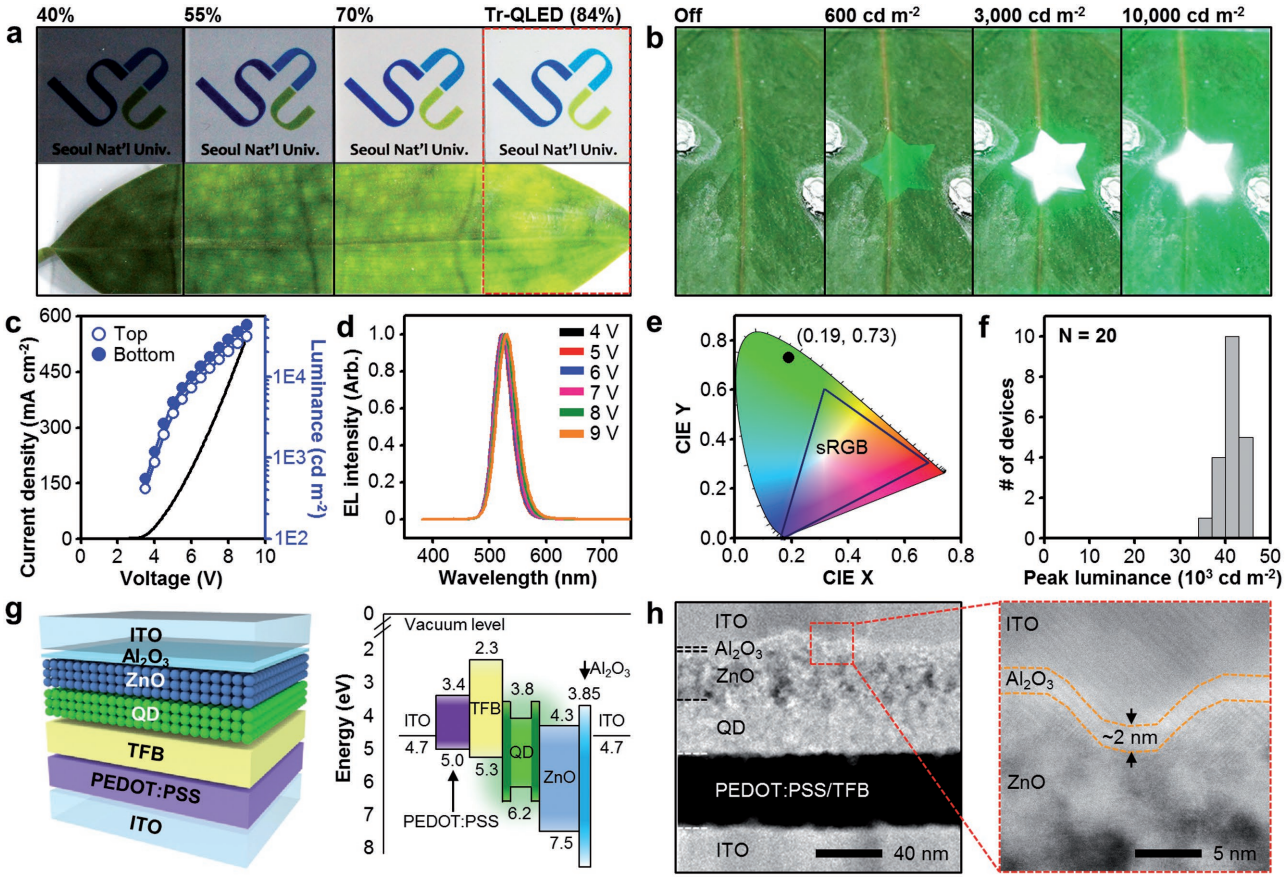

Figure 1. Extremely vivid, highly transparent quantum dot light emitting diode. a) Effect of transparency on visibility of background: the university logo (top) and a leaf (bottom). b) Effect of brightness on vividness of the display under ambient light. c) *J*–*V*–*L* characteristics, d) EL spectra, and e) CIE 1931 *x*–*y* chromaticity diagram of Tr-QLEDs. f) Histogram of peak luminance of Tr-QLEDs ($N = 20$). g) Schematic illustration of the device structure (left) and energy-band diagram (right) of the Tr-QLED. The band edges are estimated by ultraviolet photoelectron spectroscopy. h) Cross-sectional scanning TEM image of the Tr-QLED (left) and magnified view of the ETL_{A_2} (right).

transparent displays on various curved objects (Figure S2c, Supporting Information) is desirable in smart wearables and AR/IoT devices.[20–24] Highly transparent and deformable displays not only improve aesthetic factors of the system design but also enable stacking of optical information.

Our Tr-QLEDs show the highest brightness (bottom emission: ≈43 000 cd m^{-2}, top emission: ≈30 000 cd m^{-2}, and total emission: ≈73 000 cd m^{-2} at 9 V) and transmittance (90% at 550 nm, 84% over visible range) among transparent LEDs reported to date (Figure 1c; Figure S1 and Table S1, Supporting Information). The Tr-QLEDs show pure green emission (Figure 1d) corresponding to the Commission Internationale de l'Eclairage coordinates (0.19, 0.73; Figure 1e), and good reproducibility of the peak luminance (Figure 1f). Unless otherwise stated, the EL characteristics of Tr-QLEDs below are based on bottom emission. Unique materials and device design strategies made it possible to achieve these excellent characteristics. The advanced device architecture for the Tr-QLED and the energy band diagram of materials are described in Figure 1g. All components are carefully selected by considering the energy level, carrier mobility, and solvent orthogonality. The layer structures are characterized by cross-sectional transmission electron microscopy (TEM; Figure 1h): hole transporting layers (HTLs; poly(3,4-ethylenedioxythiophene):poly(styrene sulfonate) (PEDOT:PSS) and poly[(9,9-dioctylfluorenyl-2,7-diyl)-*co*-(4,4′-(*N*-(4-sec-butylphenyl)diphenylamine))] (TFB); 20 nm each), colloidal QD emitters (40 nm), and electron transport layers (ETLs) (ZnO nanoparticles (33 nm) with alumina overlayer (2 nm)) between the indium tin oxide (ITO) anode and cathode (100 nm each). The detailed fabrication process is described in the Supporting Information.

The remarkable EL performance and transparency are attributed to the newly designed ETL (ETL_{A_x}: defined as ZnO nanoparticle assemblies with alumina overlayers of x nm thickness), which enables application of the top ITO electrode without sacrificing the device performance and balances electron/hole injection into QD emitters. The alumina overlayer is formed by oxidation of a thermally evaporated ultrathin Al layer on the ZnO nanoparticle assembly. Scanning TEM (annular bright field mode and energy dispersive X-ray spectroscopy mode) and X-ray photoelectron spectroscopy analysis confirm successful formation of the conformally overlaid alumina layers (Figure S3, Supplementary Information). The use of ITO as a top electrode leads to outstanding transparency of 84% in the

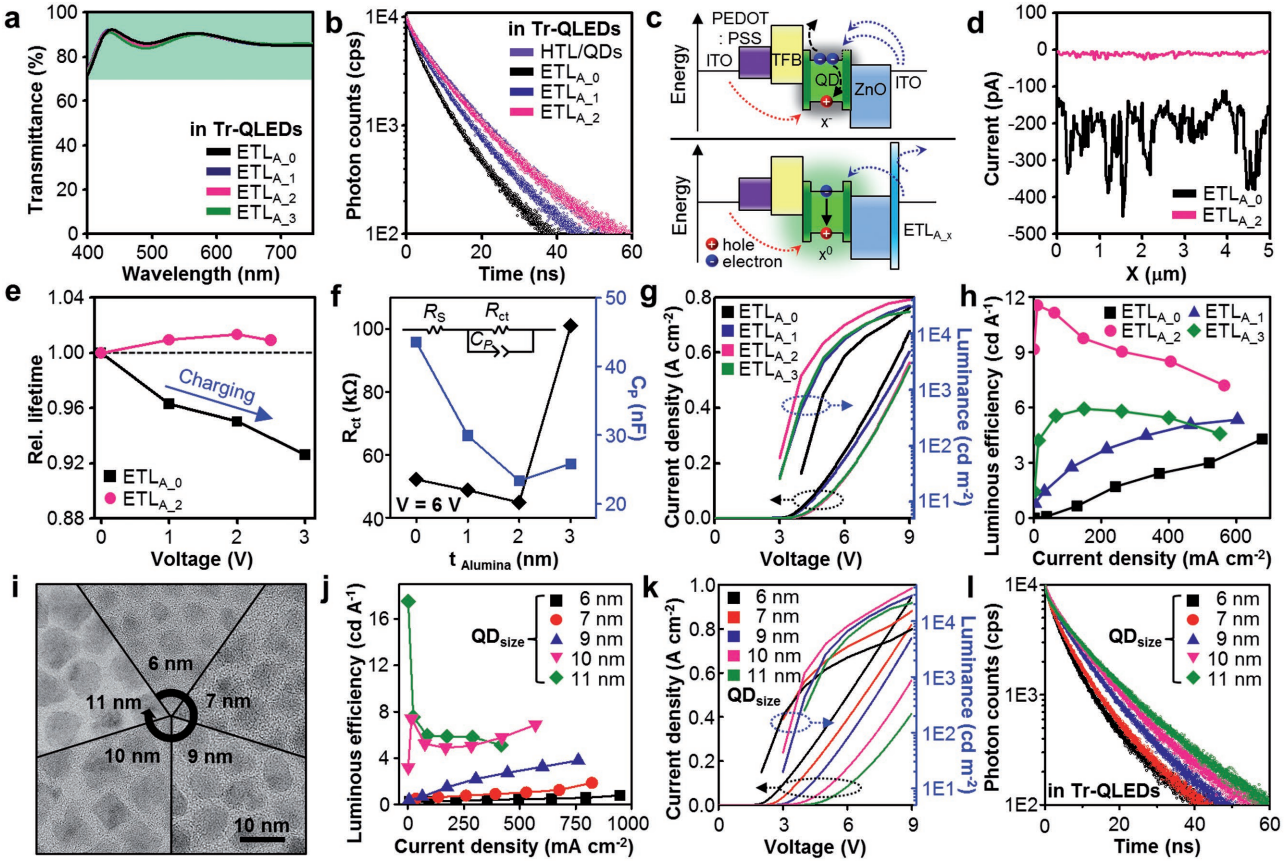

Figure 2. Optimization and characterization of ETLs and QDs for Tr-QLEDs. a) Transmittance spectra of Tr-QLEDs with the ETL_{A_x}. b) Time-resolved PL spectra of QDs in Tr-QLEDs with respect to the ETL_{A_x}. c) Schematic illustration showing the balanced carrier injection in Tr-QLEDs with the ETL_{A_x}. d) Current distribution of the ETL_{A_x} characterized by conductive AFM. e) Exciton carrier lifetime of QDs in Tr-QLEDs with ETL_{A_0} and ETL_{A_2} as a function of the applied voltage. f) Charge transport resistance (R_{ct}; left axis) and capacitance (C_P; right axis) of the Tr-QLEDs at 6 V with respect to the alumina thickness. Inset shows the equivalent circuit model. g) *J–V–L* characteristics and h) luminous efficiency of Tr-QLEDs with respect to the ETL_{A_x}. i) TEM images of core–shell QDs with different shell thicknesses. j) Luminous efficiency and k) *J–V–L* characteristics of the Tr-QLEDs employing QDs with different shell thicknesses. l) Time-resolved PL spectra of core–shell QDs with different shell thicknesses in Tr-QLEDs.

visible range (400–700 nm) and 90% at 550 nm (**Figure 2**a). The change in transmittance as stacking the composing layers of the Tr-QLED is shown in Figure S4 (Supporting Information). By using the highly transparent top ITO electrode (>90%) and the ultrathin alumina overlayer of ETL_{A_2} (≈99%), the improved device performance was achieved while maintaining the high transmittance.

To investigate the protective role of the ETL_{A_x} during the top electrode deposition, we exposed the ETL_{A_x}-coated QD films to Ar plasma (30 W, 13 Pa). The photoluminescence (PL) intensity of QDs with the ETL_{A_2} (ZnO nanoparticle assemblies with the 2 nm alumina overlayer) is preserved under the plasma treatment, while that of QDs with the ETL_{A_0} (ZnO nanoparticle assemblies) is significantly decreased (Figure S5a, Supporting Information). Time-resolved PL (TRPL) analysis of QDs within the full device also supports this protective effect of the ETL_{A_2} (Figure 2b). The carrier lifetime of QDs without the overlayer is smaller than that of QDs with ETL_{A_2} (Figure S5b, Supporting Information) because of the nonradiative defect-induced transition caused by mechanical damages. Additionally, a simple diode test also supports the protective role of ETL_{A_x} (Figure S6, Supporting Information). The device lifetime of Tr-QLEDs is measured to verify the effect of ETL modification. Without ETL modification (ETL_{A_0}), more than half of fabricated devices are short-circuited and show poor device performance due to physical and/or chemical damages during the top electrode deposition procedure. As a result, the device lifetime with ETL_{A_0} is very short, less than 1 h at 1500 cd m^{-2}, and the device lifetime variation between devices is large. On the other hand, as shown in Figure S7 of the Supporting Information, the lifetime of the Tr-QLED with ETL_{A_2} is about 23.8 h at 3.4 mA applied current (I_0 = 1509 cd m^{-2}), which corresponds to the device lifetime of 1395 h at 100 cd m^{-2} (lifetime × $I_0^{1.5}$ = const.). This value is at least 2 orders higher than the Tr-QLEDs with ETL_{A_0}, which indicates that ETL_{A_2} can prevent the plasma damage and enhance the device performance.

In addition to the protection role, the ETL_{A_x} balances electron/hole injection into QDs, which is critical for efficient radiative recombination.[25–27] Figure 2c illustrates the suggested charge transport mechanism with the ETL_{A_x}. The exciton states of QDs are easily charged by excess electrons because the electron mobility of the ZnO nanoparticle assembly is one

order of magnitude higher than the hole mobility of TFB. This induces nonradiative recombination pathways associated with the Auger process,[28,29] causing efficiency roll-off (Figure 2c, top). The ETL_{A_x}, however, prevents excessive electron injection coming from the cathode (Figure 2c, bottom). This does not affect the electron transfer between QDs and ZnO nanoparticles, since the alumina overlayer is located between ZnO nanoparticles and the cathode. Furthermore, the ETL_{A_x} significantly enhances areal homogeneity of the current distribution (Figure 2d) without affecting the surface topology (Figure S8, Supporting Information). In conductive atomic force microscopy (AFM) analysis, several spikes of the current are observed in the ETL_{A_0}, which can cause short-circuiting within the device, while the ETL_{A_2} exhibits uniform current distribution without such current spikes (Figure S9, Supporting Information).

To examine the effect of the ETL_{A_x} on the carrier dynamics, the TRPL spectra of QDs in Tr-QLEDs were measured under applied biases (Figure S10, Supporting Information).[30] Without the alumina overlayers, the QD carrier lifetime progressively decreases under the applied bias because of the increasing contribution of charged states (Figure 2e). In contrast, PL decay with the ETL_{A_2} is unaffected by the applied bias, suggesting that the modified ETL preserves charge neutrality of QDs during the device operation. This highlights that balanced hole/electron injection and controlled carrier recombination are more important than simply enhancing the carrier injection rate. In addition, electrochemical impedance analysis reveals that the ETL_{A_x} not only balances injection of electrons/holes but also enhances the charge kinetics of the device despite using insulating overlayers (Figure 2f; Figure S11, Supporting Information). The charge transport resistance (R_{ct}) and capacitance (C_p) are obtained by the equivalent circuit model (Figure 2f, inset). Tr-QLEDs with the overlayers (except the thickest one) show the low R_{ct} and C_p, particularly with the ETL_{A_2} (Figure 2f; at 6 V). The changes in C_p and R_{ct} depending on the applied voltage (Figure S11c,d, Supporting Information) imply that the overlayer with optimized thickness effectively suppresses device charging and enhances the charge transport. See Section S2.2 and Figure S11 in the Supporting Information for more detailed explanation and data.

The EL performance is dramatically improved by the ETL_{A_2} (Figure 2g,h). The luminance and efficiency of Tr-QLEDs are enhanced by optimizing the overlayer thickness, while the turn-on voltage of the Tr-QLEDs remains similar (Figure 2g,h). Note that Tr-QLEDs with the optimized ETL (i.e., ETL_{A_2}) present remarkable luminance (≈43 000 cd m^{-2} at 9 V; bottom emission) and low turn-on voltage (≈3 V) without luminance roll-off, which is attributed to the protection of active layers and balanced charge-injection into QDs. Tr-QLEDs with ETL_{A_3} show decreased luminance and luminance efficiency, because the thick alumina overlayer acts as an insulation layer and restricts electron transfer from the cathode. Conventionally, plasma enhanced atomic layer deposition (PEALD) has been used to fabricate ultrathin metal oxide layer. However, introduction of PEALD-based alumina overlayer decreases the device performance of Tr-QLEDs, because the plasma-based atomic layer deposition procedure causes damages to the QD emitters (Figure S12, Supporting Information). Therefore, we introduce the ultrathin alumina overlayer through oxidation of thermally evaporated aluminum.

Another effort to improve the EL performance is structural engineering of QDs.[31–36] We prepared a series of alloyed core/shell CdSe/ZnS QDs by growing ZnS shells of different thicknesses, which show high color purity (full width at half maximum (FWHM) of ≈30 nm) and PL quantum yield (>80%) (see Figure S13 and Section Methods of the Supporting Information for detailed synthetic procedures). The QD size is measured by TEM images (6, 7, 9, 10, and 11 nm; Figure 2i; Figure S13a, Supporting Information) and confirmed by elemental mapping images (Figure S13b, Supporting Information). In contrast to general cases, the QD bandgaps slightly increase as the shell thickness increases (Figure S13d, Supporting Information). This implies formation of alloyed core–shell interfaces by atomic interdiffusion during high-temperature shell growth, which is beneficial for effective carrier injection into QDs.[37]

The QD structure engineering significantly enhances stability of QD films (Figure S13e, Section S2.3, Supporting Information) and performance of Tr-QLEDs (Figure 2j). As the shell thickness increases, the Tr-QLEDs show reduced current density and high turn-on voltage because the thick shell acts as a charge injection barrier (Figure 2k). Meanwhile, nonradiative recombination of QDs in Tr-QLEDs (e.g., Auger recombination) is suppressed as the shell thickness increases as shown in TRPL data (Figure 2l; Figure S13f, Supporting Information). With this compensation, brightness is maximized with 10 nm QDs and total external quantum efficiency (EQE) reaches to 10% (bottom: ≈6%, top: ≈4%) with 11 nm QDs. For the optimization, we also varied the thickness of QD layer (Figure S14a, Supporting Information). As the QD thickness decreases from 45 to 34 nm, Tr-QLEDs show lower turn-on voltage and higher luminance. In addition, ligands of QDs are also optimized for the high performance Tr-QLEDs (Figure S14b, Section S2.4, Supporting Information). Based on these optimizations, we employed oleic acid-capped 10 nm QDs for Tr-QLEDs because of their high brightness.

The ultrathin form factor of Tr-QLEDs (2.7 μm total thickness; **Figure 3**a) allows high deformability,[38,39] which enables transparent displays on various curved objects.[40,41] The 330 nm thick Tr-QLED is designed to be located near the neutral mechanical plane between 1.2 μm thick parylene/epoxy double-layered encapsulation (Figure S15, Supporting Information). This design effectively minimizes the induced strain under mechanical deformations (e.g., bending, folding, and wrinkling) without any efficiency roll-off (Figure 3b–e; Movie S1, Supporting Information). Moreover, the 1.2 μm thick double-layered encapsulation shows low water vapor permeability (0.07 g mm m^{-2} d^{-1}) and oxygen permeability (0.6 cc mm m^{-2} d^{-1}), which indicates effective protection of the ultrathin Tr-QLEDs from potential water/oxygen damages. The performance of ultrathin Tr-QLEDs is highly stable regardless of the bending radius (Figure 3c) and after 1000 bending cycles (Figure 3d). Introducing the wavy structure (buckles of ≈360 μm wavelength and ≈100 μm amplitude; Figure S16a–c, Supporting Information) provides mechanical advantages, leading to an effective level of stretchability (Figure 3e). As shown in Figure S16d of the Supporting Information, the radius of curvature of the wavy structure in Tr-QLEDs (0% strain) ranges from a few micrometers to hundreds of micrometers. The peak strain in stretchable Tr-QLEDs

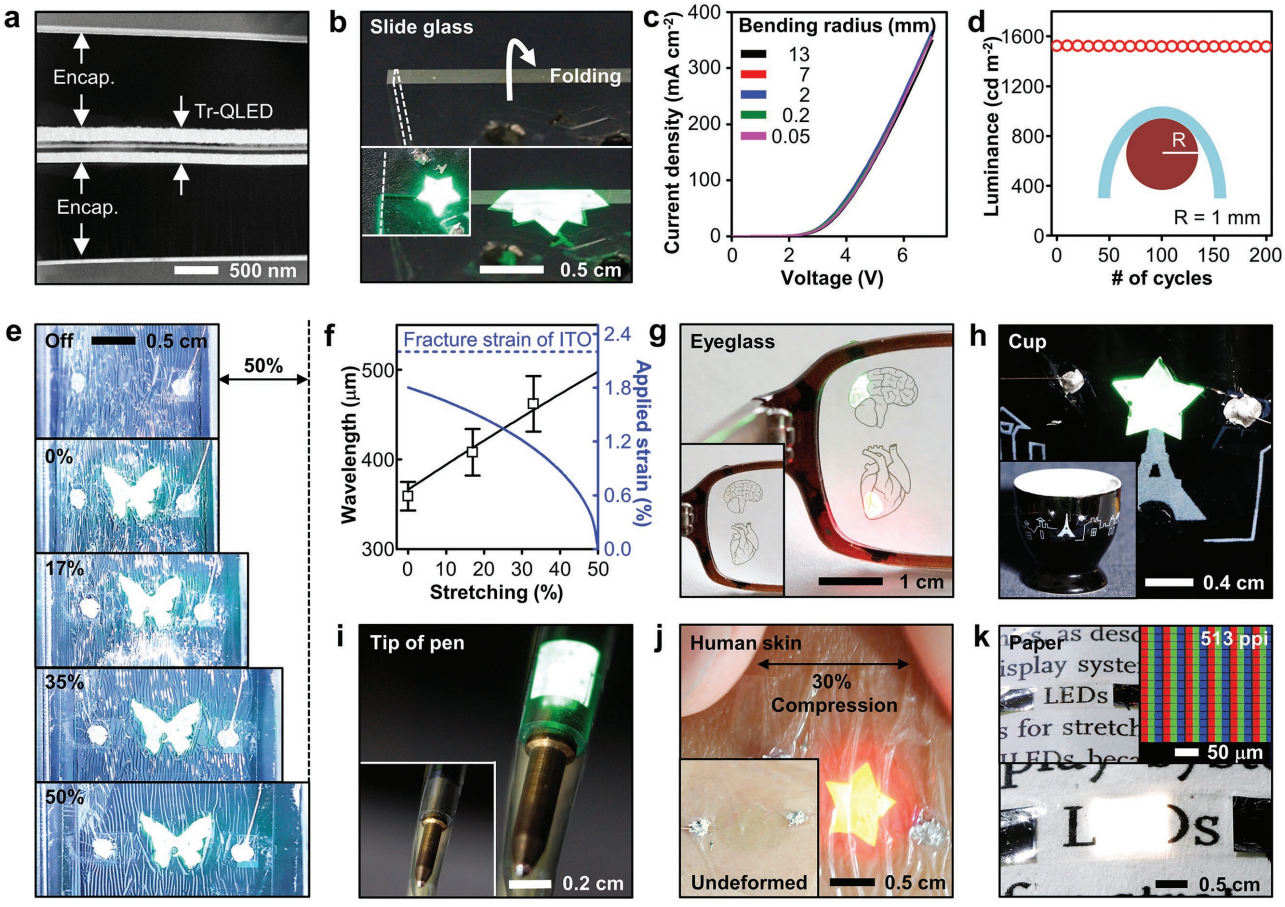

Figure 3. Ultrathin Tr-QLEDs and deformable characteristics. a) Cross-sectional TEM image of the ultrathin Tr-QLED. b) Ultrathin Tr-QLEDs folded on the edge of a slide glass. c) *J*–*V* characteristics at various bending radii. d) Durability test of the ultrathin Tr-QLED. Inset shows the bending radius (R = 1 mm). e) Ultrathin deformable Tr-QLEDs which is sequentially stretched up to 50% without any luminance changes. f) Changes in the wavelength and maximum strain of Tr-QLEDs with the applied tensile strain. g–i) Ultrathin Tr-QLEDs laminated on various curved substrates; Tr-QLEDs on eyeglasses (g), a cup (h), and the tip of a pen (i). Inset of each figure shows the off-state of Tr-QLEDs. j) Deformed Tr-QLEDs (30% compression) on human skin. Inset shows the off-state of undeformed Tr-QLEDs. k) White Tr-QLEDs based on a RGB Tr-QLED array. The array is patterned by the intaglio transfer printing method (513 pixels in^{-1}) and laminated on the paper. Inset shows the off-state of white Tr-QLEDs (left) and magnified PL image of RGB pixels (right).

is predicted to be less than the fracture strain of ITO (≈2.2%) through analytical modeling (Section S2.5, Supporting Information). When the stretchable Tr-QLED is subjected to tension, the peak strain in the device decreases with the applied tensile strain as it is a wrinkle-releasing process (Figure 3f). Consequently, the device can be deformed without any luminance decrease even after stretching up to 50% (Figure 3e).

With this outstanding deformability, Tr-QLEDs can be seamlessly integrated on objects of various curvatures (e.g., eyeglasses, a ball, a tip of a pen, a car window, a glass, and a cup; Figure 3g–i; Figure S17, Supporting Information) without affecting the original appearance or functionality of the object. For instance, Figure 3g shows bicolored Tr-QLEDs mounted on eyeglasses; such eyeglasses with integrated Tr-QLEDs can support surgeons by displaying the patient's medical information overlaid on the surgical site (e.g., vital signs, X-ray images, and computed tomography (CT)/magnetic resonance imaging (MRI) scans) and increase surgical efficiency during operations. The ultrathin Tr-QLED can be conformally integrated even on the human skin, which is an extreme case of the soft, curved, and deformable surface (Figure 3j). In addition, Tr-QLEDs with precisely aligned red, green, and blue (RGB) pixels with a resolution of 513 pixels $in.^{-1}$ are successfully fabricated using the transfer-printing technique (Figure 3k).[38,42,43] The high resolution pattering of ultrathin RGB Tr-QLEDs exhibits the potential for the deformable full-color transparent display.[44,45]

This work presents highly bright and transparent QD-LEDs with an ultrathin form factor and high color purity. The Tr-QLED performance is dramatically enhanced by engineering the ETL and QD structure. The ETL, which consists of a thin alumina layer over the ZnO nanoparticle assembly, provides protection to active layers and balances carrier injection into QDs. These device and material innovations lead to superior luminance (bottom: ≈43 000 cd m^{-2}, top: ≈30 000 cd m^{-2}, total: ≈73 000 cd m^{-2} at 9 V) and extreme transparency (90% at 550 nm, 84% over the visible range). Ultrathin nature of the transparent display (thickness: 2.7 μm) allows its conformal integration on various curved objects. The devices also maintain

the stable performance under a wide range of deformation modes (bending, folding, and stretching). This Tr-QLED technology would expedite the development of next-generation electronics including AR, IoT, and wearable devices.

Experimental Section

A detailed description of procedures and characterization methods are available in the Supporting Information. To conduct the experiment using skin-attachable devices on human skin, informed consent from the subjects to participate in the experiment was obtained and no permission was required from the institute.

Supporting Information

Supporting Information is available from the Wiley Online Library or from the author.

Acknowledgements

M.K.C., J.Y. and D.C.K. contributed equally to this work. This research was supported by IBS-R006-D1 and IBS-R006-A1. This work was also supported by a Seoul National University Research Grant.

Conflict of Interest

The authors declare no conflict of interest.

Keywords

light-emitting diodes, quantum dots, transparent displays, ultrathin electronics, wearable electronics

Received: June 12, 2017
Revised: September 2, 2017
Published online: October 25, 2017

[1] C. W. Hsu, B. Zhen, W. Qiu, O. Shapira, B. G. DeLacy, J. D. Joannopoulos, M. Soljačić, *Nat. Commun.* **2014**, *5*, 3152.
[2] P. Jing, W. Ji, Q. Zeng, D. Li, S. Qu, J. Wang, D. Zhang, *Sci. Rep.* **2015**, *5*, 12499.
[3] H. Kim, E. Brueckner, J. Song, Y. Li, S. Kim, C. Lu, J. Sulkin, K. Choquette, Y. Huang, R. G. Nuzzo, J. A. Rogers, *Proc. Natl. Acad. Sci. USA* **2011**, *108*, 10072.
[4] E. Downing, L. Hesselink, J. Ralston, R. Macfarlane, *Science* **1996**, *273*, 1185.
[5] C. Wang, D. Hwang, Z. Yu, K. Takei, J. Park, T. Chen, B. Ma, A. Javey, *Nat. Mater.* **2013**, *12*, 899.
[6] X. Dai, Y. Deng, X. Peng, Y. Jin, *Adv. Mater.* **2017**, *29*, 1607022.
[7] M. K. Choi, I. Park, D. C. Kim, E. Joh, O. K. Park, J. Kim, M. Kim, C. Choi, J. Yang, K. W. Cho, J.-H. Hwang, J.-M. Nam, T. Hyeon, J. H. Kim, D.-H. Kim, *Adv. Funct. Mater.* **2015**, *25*, 7109.
[8] H. Y. Kim, Y. J. Park, J. Kim, C. J. Han, J. Lee, Y. Kim, T. Greco, C. Ippen, A. Wedel, B.-K. Ju, M. S. Oh, *Adv. Funct. Mater.* **2016**, *26*, 3454.
[9] W. Wang, H. Peng, S. Chen, *J. Mater. Chem. C* **2016**, *4*, 1838.
[10] J. Meyer, T. Winkler, S. Hamwi, S. Schmale, H.-H. Johannes, T. Weimann, P. Hinze, Q. Kowalsky, T. Riedl, *Adv. Mater.* **2008**, *20*, 3839.
[11] J. Liang, L. Li, X. Niu, Z. Yu, Q. Pei, *Nat. Photonics* **2013**, *7*, 817.
[12] V. Wood, M. J. Panser, J.-M. Caruge, J. E. Halpert, M. G. Bawendi, V. Bulović, *Nano Lett.* **2010**, *10*, 24.
[13] T. Zhao, E. D. Goodwin, J. Guo, H. Wang, B. T. Diroll, C. B. Murray, C. R. Kagan, *ACS Nano* **2016**, *10*, 9267.
[14] C. R. Kagan, E. Lifshitz, E. H. Sargent, D. V. Talapin, *Science* **2016**, *353*, aac5523.
[15] Z.-K. Tan, R. S. Moghaddam, M. L. Lai, P. Docampo, R. Higler, F. Deschler, M. Price, A. Sadhanala, L. M. Pazos, D. Credgington, F. Hanusch, T. Bein, H. J. Snaith, R. H. Friend, *Nat. Nanotechnol.* **2015**, *9*, 687.
[16] J.-Y. Kim, J. Yang, J. H. Yu, W. Baek, C.-H. Lee, H. J. Son, T. Hyeon, M. J. Ko, *ACS Nano* **2015**, *9*, 11286
[17] J.-K. Song, D. Son, J. Kim, Y. J. Yoo, G. J. Lee, L. Wang, M. K. Choi, J. Yang, M. Lee, K. Do, J. H. Koo, N. Lu, J. H. Kim, T. Hyeon, Y. M. Song, D.-H. Kim, *Adv. Funct. Mater.* **2017**, *27*, 1605286.
[18] V. L. Colvin, M. C. Schlamp, A. P. Alivisatos, *Nature* **1994**, *370*, 354.
[19] Y. Shirasaki, G. J. Supran, M. G. Bawendi, V. Bulović, *Nat. Photonics* **2013**, *7*, 13.
[20] T. Yokota, P. Zalar, M. Kaltenbrunner, H. Jinno, N. Matsuhisa, H. Kitanosako, Y. Tachibana, W. Yukita, M. Koizumi, T. Someya, *Sci. Adv.* **2016**, *2*, e1501856.
[21] M. S. White, M. Kaltenbrunner, E. D. Głowacki, K. Gutnichenko, G. Kettlgruber, I. Graz, S. Aazou, C. Ulbricht, D. A. M. Egbe, M. C. Miron, Z. Major, M. C. Scharber, T. Sekitani, T. Someya, S. Bauer, N. S. Sariciftci, *Nat. Photonics* **2013**, *7*, 811.
[22] T. Sekitani, H. Nakajima, H. Maeda, T. Fukushima, T. Aida, K. Hata, T. Someya, *Nat. Mater.* **2009**, *8*, 494.
[23] Y. Wang, C. Zhu, R. Pfattner, H. Yan, L. Jin, S. Chen, F. Molina-Lopez, F. Lissel, J. Liu, N. I. Rabiah, Z. Chen, J. W. Chung, C. Linder, M. F. toney, B. Murmann, Z. Bao, *Sci. Adv.* **2017**, *3*, e1602076.
[24] D. Son, S. I. Chae, M. Kim, M. K. Choi, J. Yang, K. Park, V. S. Kale, J. H. Koo, C. Choi, M. Lee, J. H. Kim, T. Hyeon, D.-H. Kim, *Adv. Mater.* **2016**, *28*, 9326.
[25] B. S. Mashford, M. Stevenson, Z. Popovic, C. Hamilton, Z. Zhou, C. Breen, J. Steckel, V. Bulovic, M. Bawendi, S. C. Sullivan, P. T. Kazlas, *Nat. Photonics* **2013**, *7*, 407.
[26] X. Dai, Z. Zhang, Y. Jin, Y. Niu, H. Cao, X. Liang, L. Chen, J. Wang, X. Peng, *Nature* **2014**, *515*, 96.
[27] D. V. Talapin, J.-S. Lee, M. V. Kovalenko, E. V. Shevchenko, *Chem. Rev.* **2010**, *110*, 389.
[28] V. I. Klimov, A. A. Mikhailovsky, D. W. McBranch, C. A. Leatherdale, M. G. Bawendi, *Science* **2000**, *287*, 1011.
[29] A. L. Efros, D. J. Nesbitt, *Nat. Nanotechnol.* **2016**, *11*, 661.
[30] N. Oh, B. H. Kim, S.-Y. Cho, S. Nam, S. P. Rogers, Y. Jiang, J. C. Flanagan, Y. Zhai, J.-H. Kim, J. Lee, Y. Yu, Y. K. Cho, G. Hur, J. Zhang, P. Trefonas, J. A. Rogers, M. Shim, *Science* **2017**, *355*, 616.
[31] Y. Yang, Y. Zheng, W. Cao, A. Titov, J. Hyvonen, J. R. Manders, J. Xue, P. H. Holloway, L. Qian, *Nat. Photonics* **2015**, *9*, 259.
[32] W. K. Bae, Y.-S. Park, J. Lim, D. Lee, L. A. Padilha, H. McDaniel, I. Robel, C. Lee, J. M. Pietryga, V. I. Klimov, *Nat. Commun.* **2013**, *4*, 3661.
[33] X. Gong, Z. Yang, G. Walters, R. Comin, Z. Ning, E. Beauregard, V. Adinolfi, O. Voznyy, E. H. Sargent, *Nat. Photonics* **2016**, *10*, 253.
[34] A. Jane, O. Voznyy, S. Hoogland, M. Korkusinski, P. Hawrylak, E. H. Sargent, *Nano Lett.* **2016**, *16*, 6491.
[35] C. R. Kagan, C. B. Murray, *Nat. Nanotechnol.* **2015**, *10*, 1013.

[36] L. Sun, J. J. Choi, D. Stachnik, A. C. Bartni, B.-R. Hyun, G. G. Malliaras, T. Hanrath, F. W. Wise, *Nat. Nanotechnol.* **2012**, *7*, 369.
[37] W. K. Bae, L. A. Padilha, Y.-S Park, H. McDaniel, I. Robel, J. M. Pietryga, V. I. Klimov, *ACS Nano* **2013**, *7*, 3411.
[38] M. K. Choi, J. Yang, K. Kang, D. C. Kim, C. Choi, C. Park, S. J. Kim, S. I. Chae, T.-H. Kim, J. H. Kim, T. Hyeon, D.-H. Kim, *Nat. Commun.* **2015**, *6*, 7149.
[39] S. Choi, H. Lee, R. Ghaffari, T. Hyeon, D.-H. Kim, *Adv. Mater.* **2016**, *28*, 4203.
[40] S. Lee, A. Reuveny, J. Reeder, S. Lee, H. Jin, Q. Liu, T. Yokota, T. Sekitani, T. Isoyama, Y. Abe, Z. Suo, T. Someya, *Nat. Nanotechnol.* **2010**, *11*, 472.
[41] S.-I. Park, Y. Xiong, R.-H. Kim, P. Elvikis, M. Meitl, D.-H. Kim, J. Wu, J. Yoon, C.-J. Yu, Z. Liu, Y. Huang, K.-C. Hwang, P. Ferreira, X. Li, K. Choquette, J. A. Rogers, *Science* **2009**, *325*, 977.
[42] L. Kim, P. O. Anikeeva, S. A. Coe-Sullivan, J. S. Steckel, M. G. Bawendi, V. Bulović, *Nano Lett.* **2008**, *8*, 4513.
[43] J. Yang, M. K. Choi, D.-H. Kim, T. Hyeon, *Adv. Mater.* **2016**, *28*, 1176.
[44] T. H. Kim, K.-S. Cho, E. K. Lee, S. J. Lee, J. Chae, J. W. Kim, D. H. Kim, J.-Y. Kwon, G. Amaratunga, S. Y. Lee, B. L. Choi, Y. Kuk, J. M. Kim, K. Kim, *Nat. Photonics* **2011**, *5*, 176.
[45] B. H. Kim, M. S. Onses, J. B. Lim, S. Nam, N. Oh, H. Kim, K. J. Yu, J. W. Lee, J.-H. Kim, S.-K. Kang, C. H. Lee, J. Lee, J. H. Shin, N. H. Kim, C. Leal, M. Shim, J. A. Rogers, *Nano Lett.* **2015**, *15*, 969.